

Error analysis for a diffraction grating interferometric stylus probing system

Kuang-Chao Fan¹, Chung-De Su¹ and Jong-I Mou²

¹ Department of Mechanical Engineering, National Taiwan University, Taipei, Taiwan, Republic of China

² Department of Industrial Engineering, Arizona State University, Tempe, AZ, USA

E-mail: fan@ccms.ntu.edu.tw

Received 23 November 2000, accepted for publication 26 January 2001

Abstract

A prototype of a stylus probe with an interferometric transducer for surface profiling and roughness measurement was recently developed for surface texture, form error, radius, inclination and dimension measurement.

A reflective cylindrical holographic diffraction grating fabricated into cylindrical shape, referred to as the 'length master', acts as the moving part governing the path length of light. The surface profile information was transformed into electrical signals using a laser diode grating interferometer to measure the rotational motion of the measuring lever. To precisely define the performance capability of the system, error analysis was performed in order to assess the potential measuring error due to imperfections in manufacturing and assembly of the system's mechanical components. The uncertainty relating to the construction of the device, geometrical features, operating environment and optical characteristics is also presented.

Keywords: error analysis, stylus probe, diffraction grating interferometry

1. Introduction

Surface metrology plays an important role in precision manufacturing. Surface topography measurements can be categorized into three forms according to the characteristics of the measuring principle, namely the stylus method, optical method and scanning microscopic method. The most popular method of surface geometry measurement is the stylus profiling technique, whereby a tipped stylus is made to glide over the workpiece and derive the profile information [1–5]. There are three major optical methods, namely phase shifting interferometry [6–8], differential interferometry [9–11] and heterodyne interferometry [12–14]. Scanning microscopic methods include SEM, TEM, STEM, STM and AFM. These systems have been adopted for nano-metrology [15, 16].

In addition to measurement of surface geometry and topography, the stylus method is being actively considered for measuring important physical properties such as friction, elasticity, nano-hardness and surface energy. Using computational techniques, simultaneous evaluation and calculation of surface texture, form error, radius, inclination and dimensions can be achieved during a single traverse over the workpiece. These techniques require applying a stylus

arm displacement transducer with a very high ($>10^4$) ratio of measuring range to resolution.

A stylus probe using an interferometric transducer that can be applied for surface texture, form error, radius, inclination and dimension measurement has recently been developed [17, 18]. The reflective cylindrical holographic diffraction (RCHD) grating interferometer that acts as the moving part governs the path length of light, referred to as the 'length master', is adopted instead of a laser interferometer [19–25]. The photo-detection system for capturing interference signals and the corresponding signal processing algorithms [26–29] have been developed. Hundredths of micrometres of resolution and a reproducibility of several millimetres measuring range are available. The advantages of the probe are that it is compact, interchangeable among measuring devices, easy to construct and inexpensive.

In this paper, the principles of the RCHD grating and the design of the profiling stylus mechanism are briefly discussed. The principles of interference fringe transformation and frequency shifting are also reviewed. An error analysis was derived in order to assess the potential measuring errors due to the imperfections in manufacturing and assembly of the system. Various uncertainties and their effects are also discussed.

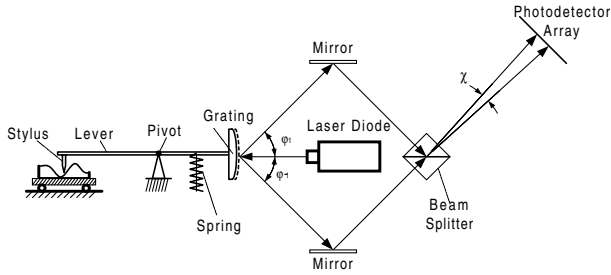


Figure 1. A schematic diagram of the stylus probing system.

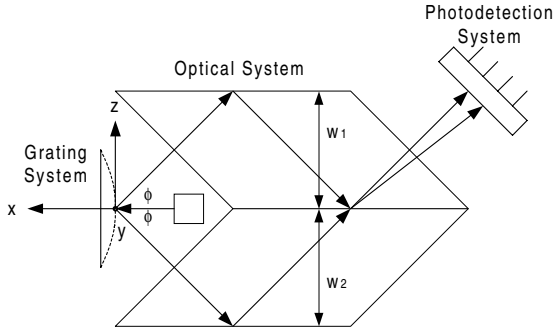


Figure 2. The RCDG grating coordinate system.

2. The components and measuring principle of the system

The key components of the system are the RCHD grating, stylus mechanism, laser diode, photodiode, interference fringe transformation algorithm and signal processing circuit.

2.1. The measuring principle of the reflecting cylindrical diffraction grating

Using a reflecting cylindrical diffraction grating (RCDG) as a component of a displacement transducer necessitates a specific design for the stylus probe. Because of the special requirement of a broad dynamic measuring range for resolution for topography, the interferometric displacement measurement system employs a RCDG transducer operating according to the principle of the Doppler effect. The general concept of the stylus probe is shown in figure 1.

The measuring lever is pivoted at the knife bearing. The spring provides recovering force for the knife bearing to maintain the centring of the lever and the measuring tip induces a stylus force. The RCDG is fixed rigidly to the end of the internal portion of the lever. The centre of the axis of curvature of the RCDG is coincident with the axis of rotation of the lever. The holographic line phase reflecting grating fabricated on the surface of the cylinder performs as the length master for the displacement transducer. Ideally, in the simplified RCDG grating coordinate, the RCDG grating lines should be parallel to the axis of the cylinder as shown in figure 2.

The grating is illuminated by the laser diode. The laser diode adopted in this study has a peak wavelength of 650 nm and 5 mW power. Through a beam splitter, the ± 1 st-order diffraction beams are superimposed onto a linear array of a photo-detector. As the measuring tip glides over the surface being tested, the stylus probe is displaced by a distance

equivalent to the change in height. The variation in height of the measuring profile results in the rotation of the lever, so the grating lines move in the direction perpendicular to the axis of the laser beam. Therefore, the grating line surface illuminated by the laser is always perpendicular to the axes of the cylinder and the laser beam. Thus, the grating can be treated as a flat surface mathematically.

A frequency shift of the ± 1 st-order diffraction beams according to the Doppler effect will occur as soon as the tip moves. The actual frequencies of the two diffraction beams can be derived as

$$f_{+1} = f_0 + \frac{v}{d_g} \quad f_{-1} = f_0 - \frac{v}{d_g} \quad (1)$$

where f_0 is the frequency of incident light, f_{+1} is the frequency of the +1st-order diffraction beam, f_{-1} is the frequency of the -1st-order diffraction beam, v is the vertical velocity of the measuring tip and grating and d_g is the grating constant.

Thus, the interference fringes created in the photo-detector array move also because of the beating frequency,

$$\Delta f = f_{+1} - f_{-1} = 2v/d_g. \quad (2)$$

The magnitude of the beating signal received by each element of the photo-detector array can be obtained as

$$\begin{aligned} I(t) &= I_1 + I_2 \cos \left(2\pi \int_0^t \Delta f dt \right) \\ &= I_1 + I_2 \cos \left(4\pi \int_0^t \Delta v dt \right) = I_1 + I_2 \cos \left(4\pi \frac{\Delta z}{d_g} \right) \end{aligned} \quad (3)$$

where t is time and the upper limit of integration is the beating signal period T , $4\pi \Delta z/d_g$ is the phase shift due to the beating signal when the Doppler effect occurs and I_1 and I_2 are the magnitudes of the dc and ac terms of the received signal, respectively.

The drift velocity of the fringe is proportional to the vertical velocity of the measuring tip. Alteration of the fringe by one period alters the beating signal for a cycle. The phase shift for a cycle is equal to 2π and the relationship of the signal and variation in geometry can be expressed as

$$2\pi = 4\pi \Delta z/d_g. \quad (4)$$

Thus, the displacement of the grating due to the movement of the measuring tip and the quantities of pulse due to the phase shift from the beating signal are correlated as $\Delta z = d_g/2$. As a result, a signal with two sine-wave periods per grating pitch is obtained from each element of the photo-detector array. The photo-detector array then converts the interference fringe pattern into a set of four sinusoidal signals that are differing in phase by $\pi/2$ relative to each other along the direction of motion detected. With appropriate signal processing circuits, the displacement can thus be appropriately measured and quantified by counting the fringe drifting and calculating the interpolation value of the sinusoidal signals to deduce the profile of a workpiece. A flow diagram of the signal processing is shown in figure 3.

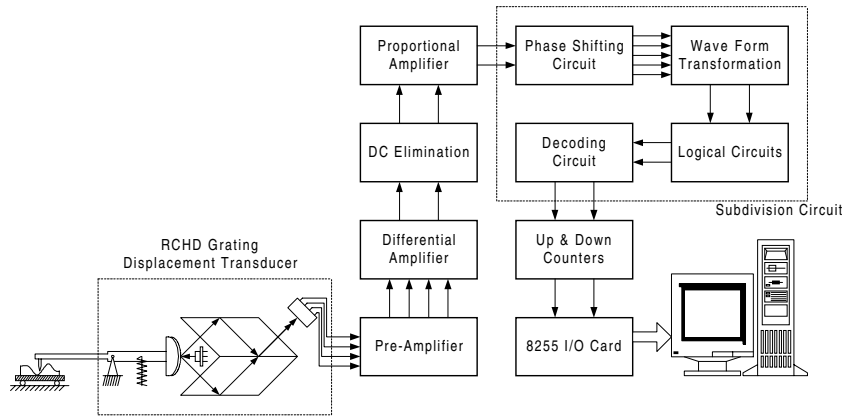


Figure 3. The flow diagram of the signal processing.

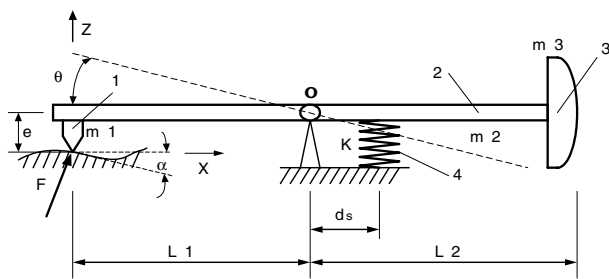


Figure 4. A schematic diagram of the stylus mechanism: 1 is the stylus, 2 is the lever, 3 is the RCHD grating, 4 is the leaf spring, d_s is the leaf spring offset distance, F is the stylus reaction force, g is the gravitational constant, K is the leaf spring constant, L_1 is the fore end length of the lever, L_2 is the rear end length of the lever, m_i is the mass of the component i ($i = 1-3$), θ is the CW rotational angle of the lever and α is the inclination of the measuring surface along the direction of the measuring path.

2.2. The design of the stylus mechanism

The requirement of a steady reaction force and robust dynamic characteristics of the profiling stylus mechanism is important. The measuring tip should surely come into contact with the surface being measured throughout a measurement. A reactive stylus force is used as a special design feature for the probe mechanism, as shown in figure 4. There are three constraints that should be satisfied.

- (i) The natural frequency of the system should be greater than the vibrational frequency of the lever during a measurement.
- (ii) The stylus force should satisfy the international standard [30].
- (iii) The eccentricity of the bearing should be minimized.

To achieve excellent centring of the bearing, the specific knife bearing method is adopted for the design of a pivot, as shown in figure 5.

2.3. The RCHD grating

The RCHD grating acts as the length master instead of the wavelength of the laser. For the manufacturing of the RCHD grating we adopt a holographic technique to fabricate it, which

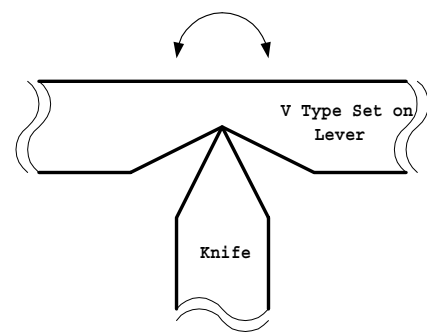


Figure 5. A schematic diagram of the knife bearing.

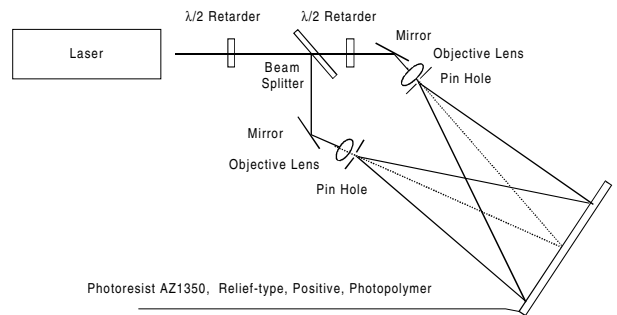


Figure 6. The scheme used for exposure.

can provide phase modulation, so that the regularly distributed interference fringe pattern is introduced as the projecting image for the emulsion on the cylindrical substrate [19–21]. The setting up and exposure of the interference fringe pattern is shown in figure 6.

2.4. The photo-detection system

A photo-detector is a sensor that converts optical energy into electrical energy via the photoelectric effect. In this study, a photodiode array is used to detect the interference fringe pattern. The distribution of the amplitude of illumination in the interference pattern along the direction perpendicular to the fringe is sinusoidal and should be tuned to fit the size of the photodiode element. To get output signals in orthogonal sinusoidal waves, the geometry of the photodiode

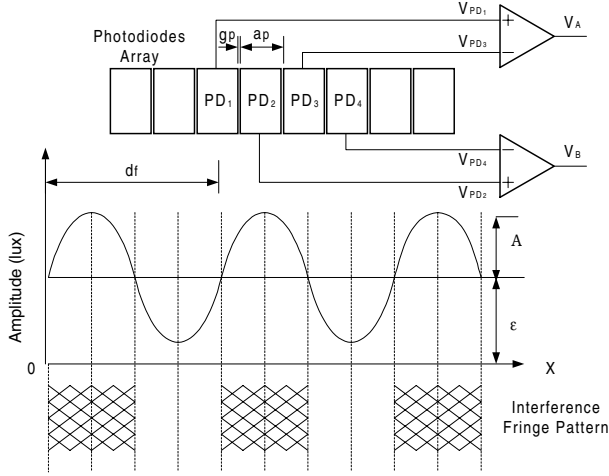


Figure 7. The scheme of the photo-detector system: ε is the illumination offset, A is the amplitude of the alternating signal, a_p is the distance between photodiodes, d_f is the fringe constant, g_p is the gap between two adjacent photodiodes and Δf is the difference between frequencies of interfering orders $+1$ and -1 .

array elements is that they are placed relative to the interference patterns in such way, shown in figure 7, that photo-detector element PD_1 detects fringe of the first order of interference.

Under the assumption that $d_f = 4a_p$ (the fringe constant is quadruple the photodiode's), the output current of each photodiode is proportional to the optical power received by each element. The photo-detector array converts the interference fringe pattern into a set of four sinusoidal signals with a phase difference of $\pi/2$.

2.5. The principle of diffraction for analysis of displacement

The major characteristics of grating interferometers that adopt diffraction gratings as length master are that they are insensitive to deviations in grating wavelength, provide a proportionally large fringe displacement relative to the actual displacement of the grating and operate independently of variations in wavelength of the light source.

When the light source encounters a rigid moving object with velocity, v , the Doppler effect of the light that is scattered by the surface of the rigid body will occur. The Doppler frequency shift of the scattering light Δf can be derived as

$$\Delta f = f_0 \left(\frac{v}{c} \right) (\cos \alpha_1 + \cos \alpha_2) \quad (5)$$

where c is the velocity of light, v is the velocity of the scattering surface, α_1 is the angle between incidence and the velocity of the scattering surface and α_2 is the angle between the velocity of the scattering surface and the observer.

The diffraction grating is used as length master for displacement measurement based on the Doppler effect of the scattering surface. Multi-frequency shifting of each order of diffraction will occur as soon as the diffraction grating moves, as shown in figure 8.

According to the Doppler effect, the frequency at point A can be determined as

$$f_A = f_0 \left(1 + \frac{v \sin \theta_1}{c} \right) \quad (6)$$

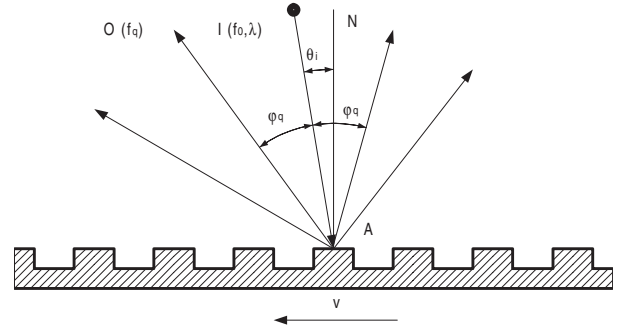


Figure 8. The Doppler effect for a moving diffraction grating. Here $I(f_0, \lambda)$ is the incident light source with initial frequency f_0 and wavelength λ and $O(f_q)$ denotes observed diffraction beams with frequency f_q .

where θ_i is the angle of incidence and v is the velocity of the diffraction grating. The q th-order frequency of reflecting diffraction is derived as

$$f_q = f_A \left(1 + \frac{v \sin \varphi_q}{c} \right) = f_0 \left(1 + \frac{v \sin \theta_i}{c} \right) \left(1 + \frac{v \sin \varphi_q}{c} \right) \quad (7)$$

where q is the order of diffraction; φ_q is the diffraction angle of the q th order. Neglecting higher order terms yields

$$\begin{aligned} f_q &= f_0 + \frac{v}{\lambda} (\sin \theta_i + \sin \varphi_q) \\ &= \frac{f_0}{c^2} [c^2 + cv(\sin \theta_i + \sin \varphi_q) + v^2 \sin \theta_i \sin \varphi_q]. \end{aligned} \quad (8)$$

Using the grating equation, one derives

$$d_g (\sin \theta_i + \sin \varphi_q) = q\lambda. \quad (9)$$

The Doppler frequency shift of the diffraction grating can be derived as

$$f_q = f_0 + \frac{v}{d_g} q = f_0 + \Delta f. \quad (10)$$

Apparently, the Doppler frequency shift of the diffraction grating is proportional to the relative velocity of the grating v , the order of diffraction q and the reciprocal of the grating constant d_g . Contrary to the usual opinion, the frequency shift is independent of the wavelength and direction of incidence.

3. Error analysis

In previous sections, the theoretical concept and design of the system developed were discussed. The performance of this system depends on the quality of the processes used to manufacture and assemble the components of the system. Any imperfection in manufacturing and assembly will cause errors when the stylus probe system is used. The measuring error is defined as the difference between a measurement and the true value. It occurs due to various factors, thus those factors should be analysed and controlled in order to minimize the measuring error.

3.1. Geometrical analysis

3.1.1. The influence of the symmetry of the mechanism. The imperfection and asymmetry of the geometrical parameters of the profiling head mechanism will induce measurement error.

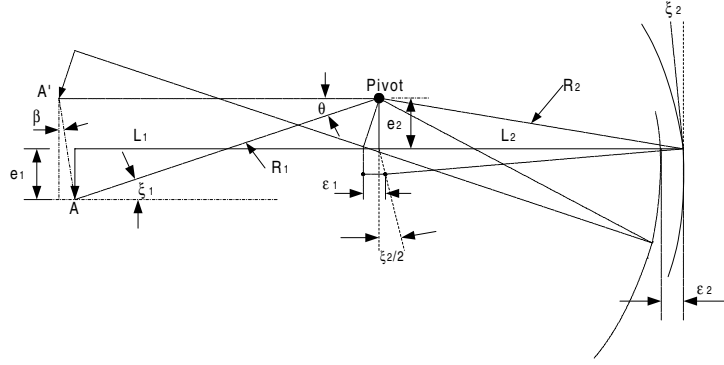


Figure 9. A schematic diagram of parameters of the mechanism.

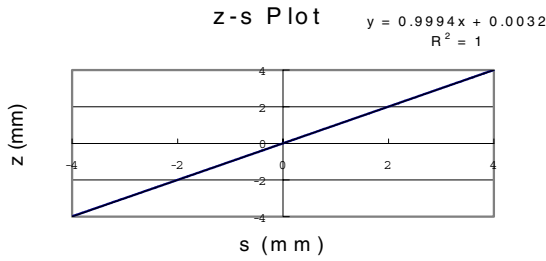


Figure 10. The relationship between grating and stylus displacements.

Thus, the parameters should be evaluated for error analysis. The mechanism with each parameter is shown in figure 9.

The tip moves from A to A' when the lever rotates by θ and the following geometrical relationships can be derived:

$$R_1 = [L_1^2 + (e_1 + e_2)^2]^{1/2} \quad (11)$$

$$R_2 = (L_2^2 + e_2^2)^{1/2} \quad (12)$$

$$\overline{AA'} = 2R_1 \sin\left(\frac{\theta}{2}\right). \quad (13)$$

Observing point A yields

$$90^\circ - \beta = 180^\circ - \xi_1 - \frac{180^\circ - \theta}{2} = 90^\circ - \xi_1 + \frac{\theta}{2} \Rightarrow \beta = \xi_1 - \frac{\theta}{2}. \quad (14)$$

The vertical displacement of the stylus tip, z , can be derived as

$$z = \overline{AA'} \cos \beta = 2(e_1 + e_2) \sin^2\left(\frac{\theta}{2}\right) + L_1 \sin \theta. \quad (15)$$

The path of motion of the grating, s , can be expressed as

$$s = R_2 \theta = (L_2^2 + e_2^2)^{1/2} \theta. \quad (16)$$

Thus, the angle of rotation θ can be derived as

$$\theta = \frac{s}{(L_2^2 + e_2^2)^{1/2}}. \quad (17)$$

Substituting (17) into (15) yields

$$z = 2(e_1 + e_2) \sin^2\left(\frac{1}{2} \frac{s}{(L_2^2 + e_2^2)^{1/2}}\right) + L_1 \sin\left(\frac{s}{(L_2^2 + e_2^2)^{1/2}}\right). \quad (18)$$

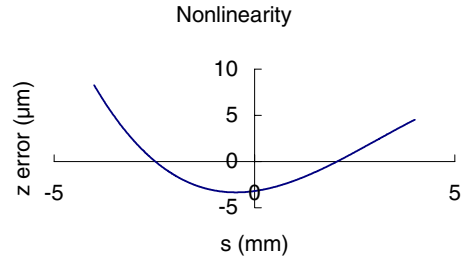


Figure 11. The non-linearity of the relative displacements.

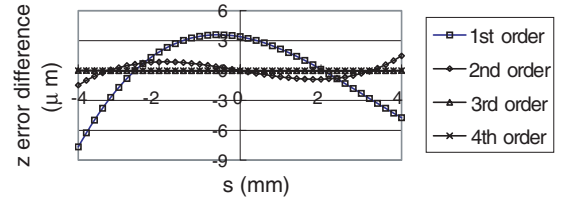


Figure 12. A plot of the difference in non-linearity.

The sensitivity of the vertical displacement z with respect to the deviation of each parameter can be expressed as

$$\frac{\partial z}{\partial e_1} = 2 \sin^2\left(\frac{1}{2} \frac{s}{(L_2^2 + e_2^2)^{1/2}}\right) \quad (19)$$

$$\frac{\partial z}{\partial e_2} = 2 \sin^2\left(\frac{1}{2} \frac{s}{(L_2^2 + e_2^2)^{1/2}}\right) - \frac{e_2 s (e_1 + e_2)}{(L_2^2 + e_2^2)^{3/2}} \sin\left(\frac{s}{(L_2^2 + e_2^2)^{1/2}}\right) - s e_2 L_1 \cos\left(\frac{s}{(L_2^2 + e_2^2)^{1/2}}\right) \quad (20)$$

$$\frac{\partial z}{\partial L_1} = \sin\left(\frac{s}{(L_2^2 + e_2^2)^{1/2}}\right) \quad (21)$$

$$\frac{\partial z}{\partial L_2} = -s L_2 (e_1 + e_2) \sin\left(\frac{s}{(L_2^2 + e_2^2)^{1/2}}\right) - \frac{s L_1 L_2}{(L_2^2 + e_2^2)^{3/2}} \cos\left(\frac{s}{(L_2^2 + e_2^2)^{1/2}}\right). \quad (22)$$

The relationship between the movement of the grating and stylus displacement can be drawn as shown in figure 10 with the following assumptions: $e_1 = 3$ mm, -0.05 mm $< e_2 < 0.05$ mm, -4 mm $< s < 4$ mm and

$L_1 = L_2 = 50 \pm 0.1$ mm. The result shows that, as $R_2 \rightarrow 1$, the non-linearity would probably be too infinitesimal to be discerned. By calculating the fitting residual and magnifying it by a factor of 1000 (in units of micrometres), the ideal non-linearity due to asymmetry of the mechanism can be presented; see figure 11.

By adopting Taylor series, equation (18) can be modified into

$$\begin{aligned}
 z(s) &= z(0) + z'(0) \frac{s}{1!} + z''(0) \frac{s^2}{2!} + z'''(0) \frac{s^3}{3!} + \dots \\
 &= 0 + \frac{L_1}{(L_2^2 + e_2^2)^{1/2}} s + \frac{e_1 + e_2}{L_2^2 + e_2^2} \frac{s^2}{2!} \\
 &\quad - \frac{L_1}{(L_2^2 + e_2^2)^{1/2}} \frac{s^3}{3!} - \frac{e_1 + e_2}{(L_2^2 + e_2^2)^2} \frac{s^4}{4!} \\
 &= L_1 \sum_{k=1}^{\infty} \frac{(-1)^{k-1} s^{2k-1}}{(L_2^2 + e_2^2)^{(3k-1)/2}} \\
 &\quad + (e_1 + e_2) \sum_{k=1}^{\infty} \frac{1}{2k!} \frac{(-1)^{k-1} s^{2k}}{(L_2^2 + e_2^2)^k}.
 \end{aligned} \tag{23}$$

Because the desired resolution is 25 nm, the difference between the non-linearity of the simplified power series $z(s)$ and the ideal non-linearity should be less than 25 nm. The least order power series should be of third order and the maximum difference between the ideal case and the third-order approximation is about 5 nm. The differences between the ideal non-linearity and each order approximation are shown in figure 12.

3.1.2. The influence of an inaccurate grating guide. While the grating moves along the direction of measurement, the inaccuracy of the grating guide causes additional shifts and tilts. These additional displacements are caused by the misalignment of the interferometric profiling head. Figure 13 shows the components of the undesired grating movement separately. The influence of each undesired shift and tilt is discussed in following subsections. Both the displacement of the grating along the x direction and the tilt of the grating around the z -axis do not affect the interference fringes; therefore, they are not analysed.

3.1.2.1. The influence of displacement in the y direction. The horizontal displacement, ε_2 , due to the rotation of the lever θ can be derived as

$$\begin{aligned}
 \varepsilon_1 = \varepsilon_2 &= \left[e_2 + 2L_2 \sin\left(\frac{\xi_2}{2}\right) \cos\left(\frac{\xi_2}{2}\right) \right] \theta \\
 &= (e_2 + L_2 \sin \xi_2) \theta.
 \end{aligned} \tag{24}$$

The optical path changes are shown in figure 14, where $\varepsilon = \varepsilon'$. Because the parameters e_2 , L_2 and φ are constant, the horizontal deviation, ε_2 , can be treated as a function that linearly depends on the rotation θ . The fringe drift in the photo-detection system can be calculated as

$$\varepsilon'' = \varepsilon \cos\left(\frac{\pi}{2}\right) = \frac{1}{\sqrt{2}} (e_2 + L_2 \sin \xi_2) \theta. \tag{25}$$

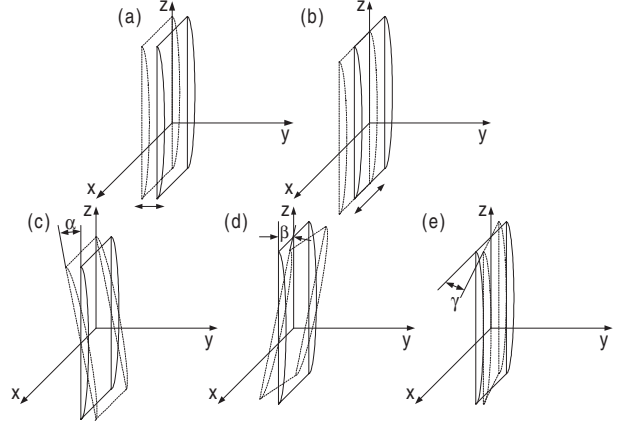


Figure 13. Components of undesired grating movement: (a) displacement in the y direction, (b) displacement in the x direction, (c) tilt around the x -axis, (d) tilt around the y -axis and (e) tilt around the z -axis.

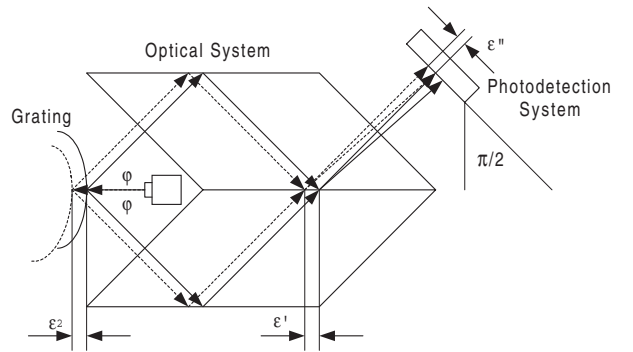


Figure 14. A diagram showing the fringe drift.

Thus, the phase drift, Φ_d , of sinusoidal signals can be derived as

$$\Phi_d = \frac{\varepsilon''}{4a_p} 2\pi = \frac{\pi(e_2 + L_2 \sin \xi_2)}{2\sqrt{2}} \theta \tag{26}$$

where a_p is the distance between photodiodes.

The phase drift due to misalignment of the mechanism linearly depends on the rotation of the lever θ . For example, if $L_2 = 50$ mm, $e_2 = 0.05$ mm, $\xi_2 = 10^\circ$ and $\theta = 10^\circ$, then $\Phi_d \cong 0.2247^\circ$.

3.1.2.2. The influence of tilt around the x -axis. The tilt of the grating by the angle α around the x -axis changes the half angle of interference by

$$\Delta\left(\frac{\chi}{2}\right) = 2\alpha. \tag{27}$$

The magnifying factor, $1/K$, can be expressed as

$$\frac{1}{K} = \frac{\Delta z'}{\Delta z} = \frac{f_z \lambda}{\sin(\chi/2)}$$

where λ is the wavelength of the incidence and f_z is the spatial frequency.

When the grating displacement is half the grating constant, $\Delta z = d_g/2$, the fringe drift $\Delta z'$ would be a period of the fringe

constant and can be derived as

$$\delta = \Delta z' = \frac{d_g}{2} \frac{f_z \lambda}{\sin(\chi/2)} = \frac{\lambda}{2 \sin(\chi/2)}. \quad (28)$$

The plane of the interfering wave vectors does not change. Thus, a change to the angle χ yields a relative change to the fringe constant derived as

$$\Delta \delta = \frac{-\lambda \cos(\chi/2)}{4 \sin^2(\chi/2)}$$

and hence

$$\frac{\Delta \delta}{\delta} = \frac{-\cos(\chi/2) \Delta \chi}{2 \sin(\chi/2)} = \frac{-\Delta \chi}{2 \tan(\chi/2)} \approx \frac{-4\alpha}{2(\lambda/2\delta)} = \frac{-4\alpha\delta}{\lambda} \quad (29)$$

where $\Delta \delta$ is the change in fringe constant and $\Delta \chi$ is the change in the angle of interference. The influence of the tilt changes the fringe constant, which means that non-orthogonality would occur in the sinusoidal signals received by the photo-detection system.

3.1.2.3. The influence of tilt around the y-axis. Tilts of the grating around the y-axis by angle β cause a similar tilting of the plane of interfering wave vectors. This tilt will also cause a deviation from orthogonality. As a result, fringes change their direction by the same angle β . Thus, the tilt of the fringes received by the photo-detection system as an increase of the fringe constant along the axis of the photo-detector is

$$d'_g = d_g / \cos \beta. \quad (30)$$

For example, if $\beta \approx 2^\circ$, $d'_g \cong 1.0006d_g$.

3.2. The effect of temperature

Although the length master used in this study is the grating constant instead of the wavelength of the light source and the quality of the laser is theoretically unimportant, the deviation in wavelength from the light source actually causes an error. According to figure 2, the normalized optical path difference (opd) can be derived as

$$opd = \frac{2w_1}{\lambda \sin \varphi} - \frac{2w_2}{\lambda \sin \varphi} = \frac{2(w_1 - w_2)}{\lambda \sin \varphi}. \quad (31)$$

Thus, the temperature sensitivity of opd can be derived as

$$\frac{\partial(opd)}{\partial T} = \frac{-2(w_1 - w_2)}{\lambda^2 \sin^2 \varphi} \left(-\cos \varphi \frac{\partial \varphi}{\partial \lambda} \frac{\partial \lambda}{\partial T} + \lambda + \sin \varphi \frac{\partial \lambda}{\partial T} \right). \quad (32)$$

According to the grating equation, the following relationships can be derived:

$$\begin{aligned} \sin \varphi &= m\lambda/d_g \\ \partial(\sin \varphi) &= \cos(\varphi) \partial \varphi = \partial \left(\frac{m\lambda}{d_g} \right) = \frac{m}{d_g} \partial \lambda \\ \frac{\partial \varphi}{\partial \lambda} &= \frac{m}{d_g \cos \varphi} = \frac{1}{d_g \cos \varphi} = c_1 \end{aligned} \quad (33)$$

where m is the phase modulation factor.

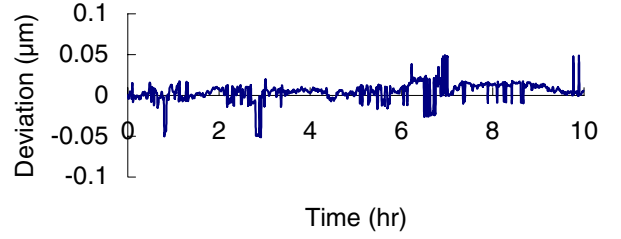


Figure 15. A plot of temperature control stability.

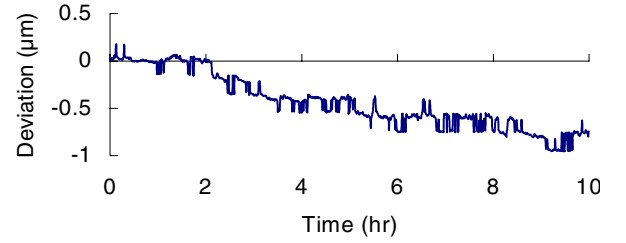


Figure 16. A plot of temperature increase stability.

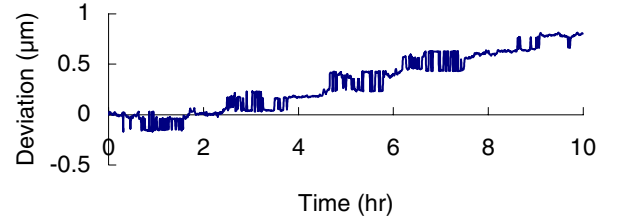


Figure 17. A plot of temperature decrease stability.

The sensitivity of the laser wavelength drift can be treated as a constant as

$$\frac{\partial \lambda}{\partial T} = c_2 \quad (34)$$

Thus, the normalized optical path difference can be expressed as

$$\begin{aligned} \Delta opd &= \frac{\partial(opd)}{\partial T} \Delta T \\ &= \frac{-2(w_1 - w_2)}{\lambda^2 \sin^2 \varphi} (-c_1 c_2 \lambda \cos \varphi + c_2 \sin \varphi) \Delta T. \end{aligned} \quad (35)$$

Δopd is linearly dependent on the temperature difference ΔT . If $w_1 = w_2$, the opd will be insensitive to the temperature deviation. However, there is a slight difference between these two dimensions, so an influence of the temperature deviation on opd is inevitable. To test the influence of the temperature deviation, a stability experiment was performed with three situations: temperature control, an increase in temperature and a decrease in temperature.

The stability test for temperature control was performed in a constant-temperature, $T = 20^\circ\text{C}$, environment. The results are shown in figure 15. The stability test for an increase in temperature was performed in a common air-conditioned laboratory from morning to afternoon. The results are shown in figure 16. The stability test for a decrease in temperature was performed in a common air-conditioned laboratory from afternoon to evening. The results are shown in figure 17.

It is observed that there would be a deviation of less than ± 50 nm under temperature control. This also means that the deviation of the system would be less than ± 2 bits in 16 subdivisions. In a common air-conditioned laboratory, there would be $1 \mu\text{m}$ drift caused by a temperature deviation (of $\pm 1.5^\circ\text{C}$) over 10 h.

3.3. Variation of the fringe constant

The influence of the deviation from orthogonality caused by a change in fringe constant that can be detected by the photo-detection system is discussed in this section. As mentioned earlier, several parameters affect the fringe constant and the influence caused by the change in fringe constant is measurable.

When the fringe constant does not satisfy the assumption $d_g = 4a_p$, the general form of the two output sinusoidal signals can be derived as

$$\begin{aligned} V_A &= V_1 - V_3 = \frac{Ad_g}{\pi} \sin(\Psi)[\sin(\Psi + 2\pi \Delta ft) \\ &\quad - \sin(5\Psi + 2\pi \Delta ft)] \\ &= \frac{-2Ad_g}{\pi} \sin(\Psi) \sin(2\Psi) \cos(3\Psi + 2\pi \Delta ft) \end{aligned} \quad (36)$$

$$\begin{aligned} V_B &= V_2 - V_4 = \frac{Ad_g}{\pi} \sin(\Psi)[\sin(3\Psi + 2\pi \Delta ft) \\ &\quad - \sin(7\Psi + 2\pi \Delta ft)] \\ &= \frac{-2Ad_g}{\pi} \sin(\Psi) \sin(2\Psi) \cos(5\Psi + 2\pi \Delta ft) \end{aligned} \quad (37)$$

where $(2Ad_g/\pi) \sin(\Psi) \sin(2\Psi)$ is the amplitude of the sinusoidal signals. The phase difference of the signals (pd) can be expressed as

$$pd = (5\Psi + 2\pi \Delta ft) - (3\Psi + 2\pi \Delta ft) = 2\Psi = 2\pi a_p/d_g. \quad (38)$$

Thus, the deviation in phase difference due to Δd_g can be presented as

$$\Delta pd = \frac{2\pi a_p}{d_g + \Delta d_g} - \frac{2\pi a_p}{d_g} = \frac{-2\pi a_p \Delta d_g}{d_g(d_g + \Delta d_g)}. \quad (39)$$

For instance, when $\Delta d_g = 10\% \times d_g$,

$$\Delta pd = \frac{-2\pi a_p d_g/10}{d_g(d_g + d_g/10)} = \frac{-2\pi a_p}{11d_g} \approx -8.19^\circ.$$

4. Conclusions

The development of a prototype of a stylus probe with an interferometric transducer for surface profiling and roughness measurement is briefly presented. Analysis of the geometrical errors and asymmetry of the mechanism was conducted. The uncertainties arising from the construction of the device, geometrical features, operating environment and optical characteristics were also presented.

To enhance the precision of the system, the influence of error factors should be properly reduced and controlled. MEMS technology could be adopted to produce an equivalent radial grating instead of the RCHD grating. Polarizing components could also be adopted in order to ensure the

orthogonality of sinusoidal signals. The deviation from orthogonality can be compensated by use of a software algorithm. If the inducements of the errors could be eliminated to infinitesimal, the resolution, linearity and stability of the system could be ensured.

References

- [1] Whitehouse D J 1998 Stylus contact method for surface metrology in the ascendancy *Meas. Control* **31** 48–50
- [2] Whitehouse D J 1997 Surface metrology *Meas. Sci. Technol.* **8** 955–72
- [3] Rank Taylor Hobson Ltd 1989 *Prospectus for Form Talysurf*
- [4] Garratt J D, Bates W J and Player M J 1981 Polarizing optical system *UK Patent Application* GB 2070276A
- [5] Garratt J D 1982 A new stylus instrument with a wide dynamic range for use in surface metrology *Precision Engng* **4** 384–9
- [6] Bruning J H, Herriott D R, Gallagher J E, Rosenfeld D P, Whit A D and Brangaccio D J 1974 Digital wavefront measuring interferometer for testing optical surface and lenses *Appl. Opt.* **13** 1235–41
- [7] Bhushan B, Wyant J C and Koptopoulos C L 1985 Measurement of surface topography of magnetic tapes by Mirau interferometry *Appl. Opt.* **24** 931–6
- [8] Ishikawa S 1992 Phase shifting interferometry with a coupled interferometer: application to optical roughness of blocks gauges *Optics* **91** 231–5
- [9] Lessor D L, Hartman J S and Gordon R L 1979 Quantitative surface topography determination by Nomarski reflection microscopy *J. Opt. Soc. Am.* **69** 189–93
- [10] Hartman J S, Gordon R L and Lessor D L 1980 Quantitative surface topography determination by Nomarski reflection microscopy, microscope modification calibration, and planar sample experiments *Appl. Opt.* **19** 1892–7
- [11] Bristow T C 1988 Surface roughness measurement over long scan lengths *Surf. Topogr.* **1** 18–23
- [12] Sommargren G E 1981 Optical heterodyne profilometry *Appl. Opt.* **20** 2675–81
- [13] Pantzer D 1987 Step response and spatial resolution of an optical heterodyne profiling instrument *Appl. Opt.* **26** 3014–19
- [14] Pantzer D, Politch J and Er L 1986 Heterodyne profiling instrument for angstrom region *Appl. Opt.* **25** 4168–72
- [15] Montaner D 1992 Surface detect analysis of semiconductor materials and devices using nanoscopy techniques *Proc. SPIE* **1776** 34–45
- [16] Glenn P 1990 Angstrom level profilometry for sub-millimetre to meter scale surface errors *Proc. SPIE* **1333** 326–36
- [17] Fan K C, Su C D and Mou J 2001 Development of high precision stylus diffraction grating interferometric probe and system: part 1—mechanism and diffraction grating design *Precision Engng* submitted
- [18] Fan K C, Su C D and Mou J 2001 Development of high precision stylus diffraction grating interferometric probe and system: part 2—signal processing and applications *Precision Engng* submitted
- [19] Dobosz M 1994 New stylus probe with interferometric transducer for surface roughness and form profiling *Opt. Engng* **33** 902–7
- [20] Dobosz M 1994 Application of a divergent laser beam in a grating interferometer for high-resolution displacement measurement *Opt. Engng* **33** 897–901
- [21] Dobosz M 1992 High-resolution laser transducer of linear displacements *Opt. Engng* **31** 500–4
- [22] Tiebang X 1989 The research and design into an intelligence instrument with holographic diffraction grating *Proc. 2nd IMECCO TC14 Int. Symp. ISMQC/IMECO* pp 296–310
- [23] Jiang Z Q, Xie T B, Yao C X and Li Zhu 1993 Grating technology for topography measurement of curve surface *Proc. SPIE* **2101** 554–7

- [24] Dobosz M 1983 Optical profilometer: a practical approximate method of analysis *Appl. Opt.* **22** 1892–7
- [25] Dobosz M 1984 Accuracy of profile measurements by means of focused laser beam *Wear* **98** 117–26
- [26] Yu Q, Andresen K and Osten W 1994 Analysis and removal of the systematic phase error in interferograms *Opt. Engng* **33** 1630–7
- [27] Pace P E and Styer D 1994 High-resolution encoding process for an integrated optical analog-to-digital converter *Opt. Engng* **33** 2638–45
- [28] Taylor H F 1975 An optical analog-to-digital converter design and analysis *IEEE J. Quantum Electron.* **15** 210–16
- [29] Chibane Y, Lamoreaux S K, Pendlebury J M and Smith K F 1995 Minimum variance of frequency estimation for a sinusoidal signal with low noise *Meas. Sci. Technol.* **6** 1671–8
- [30] Deutsche Norm 1979 *Elektrische Tastschnittgeräte zur Messung der Oberflächenrauhe nach dem Tastschnittverfahren* (Berlin)